2013 IEEE 10th International Symposium on Biomedical Imaging:
From Nano to Macro
San Francisco, CA, USA, April 7-11, 2013

SEGMENTATION AND SURFACE RECONSTRUCTION MODEL OF PROSTATE MRI TO IMPROVE PROSTATE CANCER DIAGNOSIS

Ruida Cheng [a], Marcelino Bernardo [b,c], Justin Senseney [a], Alexandra Bokinsky [d], William Gandler [a], Baris Turkbey [c], Thomas Pohida [a], Peter Choyke [c], Matthew J. McAuliffe [a]

[a] Image Science Laboratory, Center of Information Technology, National Institutes of Health, Bethesda, MD
[b] Molecular Imaging Program, National Cancer Institute, Bethesda, MD
[c] SAIC-Frederick, Frederick National Laboratory, Frederick, MD
[d] Geometric Tools, Inc. Chapel Hill, NC

ABSTRACT

This work presents a MRI prostate segmentation and surface reconstruction model that facilities the validation of multi-parametric MRI with histopathology slides from radical prostatectomy specimens and targeted biopsy specimens. Application of this technique combines image processing and computer aided design to provide a generalized solution to construct a high resolution 3D prostate surface from MRI images in three orthogonal views with non-isotropic voxel resolution. The performance of the segmentation is evaluated with 45 MR image datasets, yielding an average segmentation accuracy of 90%.

Keywords **—** Prostate Segmentation, Registration, Surface Reconstruction

1. INTRODUCTION

The use of multi-parametric MRI to localize a patient's prostate cancer has the potential to improve clinical diagnosis and staging. To realize this, the segmentation of the prostate gland boundary from three-dimensional magnetic resonance imaging (MRI) to generate a surface model is essential. Shah *et al*. used patient-specific molds (PSM) created from prostate surface models to correlate MRI to histopathology and develop a decision support system for generating cancer probability maps from multi-parametric MRI [1]. The PSM is created using prostate surface models from MR images of each patient obtained prior to surgery. The prostate margin segmentation was performed manually. Since the multi-slice MRI scans were obtained with thick slices relative to the in-plane resolution due to scan time constraints, a surface model generated from only one view, such as axial view, gave poor resolution in the slice direction. For the PSM, this was improved by segmenting the prostate in three orthogonal MRI scans and combining them either as binary masks or as cloud of points before reconstructing the surface. The same prostate surface model could also be used in another method to validate MRI with histopathology where multi-parametric MRI is fused to trans-rectal ultrasound (TRUS) in order to target lesions during biopsy [2]. A semi-automated segmentation and surface reconstruction approach would reduce the amount of tedious manual labor needed to process the multiple multi-slice images.

In previous work, few methods were proposed for MRI prostate segmentation and surface reconstruction. Betrouni *et al.* proposed a 3D deformable model [3], which utilizes Iterative Closest Point (ICP) algorithm and Principle Component Analysis (PCA) to deform 3D prostate contour points and to reach the final segmentation result. A fuzzy set algorithm is used to reconstruct the 3D prostate surface based on slice profile. Dowling *et al.* proposed a specific deformable model [4] consisting of a patient specific initialized triangulated surface and image feature model that are trained during initialization. The image feature model is used to deform the initialized surface by template matching image features via normalized cross-correlation to the features of scan. The final surface is obtained via well-established simple surface smoothing algorithms. Yin *et al*. proposed an automated segmentation model [5] based on normalized gradient field cross-correlation for initialization, and graph-search based framework for refinement. The method deformed a mean-shape prostate shape mesh to the desired prostate shape in segmentation process. The mean shape mesh was generated from ground truth training label images using the marching cubes algorithm.

As compared to those existing deformation and learning based prostate segmentation and surface reconstruction algorithms, we propose a novel method that utilizes 1) reliable gradient descent B-Spline registration to segment prostate MRI, 2) robust Ball-pivoting and Poisson algorithms to extract high resolution surface from thick-sliced MRI.

2. METHODS

The proposed model is described in three major building blocks: 1) Semi-automatic B-Spline registration-guided

segmentation model using MRI prostate images, and 2) Ball-pivoting and Poisson based 3D surface reconstruction. We present each component in the following subsections. The schema of the proposed model is shown in Figure 1.

The input data are MR images, which are obtained from a 3.0 T whole-body MRI system (Achieva, Philips Healthcare). T_2-weighted MR images of the entire prostate were obtained in three orthogonal planes (sagittal, axial and coronal) at the scan resolution of 0.2734x0.2734x3.0 mm^3; field of view 140 mm; image slice dimension 512x512. The center of the prostate is the focal point for MRI scan. To reduce the scan time, a lower refocusing pulse of 100 degrees was used for sagittal and coronal images, which alters the contrast on these images compared to the axial images.

2.1. Multi-threaded B-Spline registration guided semi-automatic prostate segmentation

During initialization, researchers manually outline three volume of interest (VOI) contours on separate slices for each axial, sagittal and coronal image to define the middle, the apex, and the base of the prostate, as shown in Figure 1. A fully automatic registration guided algorithm concurrently executes the prostate segmentation to all three orthogonal images. The algorithm proceeds from the midsection slice to the adjacent slices and then iteratively propagates toward the specified apex and base contours. Near the two ends, apex and base contours start as the initial estimate, propagating towards the ending slices. The procedure that leads to a segmentation result is based on registering neighboring slices.

The proposed model uses 2D registration to register 2D slices from the middle slice to the adjacent slice. It then generates a new VOI contour, and takes the VOI as the new initial estimate for the next slice in the series. This process is then iteratively propagated in both forward and backward directions. A fully automated segmentation model is demonstrated in Figure 2. The model diagram is a single thread processing pipeline that executes on each acquired image. The four major steps are: 1) The original prostate MR image is cropped into a smaller image according to the specified middle slice VOI; 2) The coherence enhancing diffusion (CED) filter is applied to the cropped MRI image to reduce the speckle-like noise and enhance the edge boundary information; 3) 2D B-Spline registration algorithm registers the two adjacent CED slices, and generates the segmented VOI on the target image slice; (4) Smooth the VOI and translate the VOI back from the cropped slice to original image slice.

Gradient descent B-Spline registration between 2D CED slices guides the automatic segmentation to find the coarse prostate boundary. It registers a 2D source image to a 2D target image (adjacent slice). A 2D B-Spline is used to map the coordinates of the registered image to the coordinates of the input source image. A separate B-Spline basis is setup for each axis given the number of control points and the degree of the basis functions to use. Each B-Spline is uniformly opened with control points spaced equally for each dimension. Bilinear interpolation is used to determine which input source image values to assign to the resulting registered source image. The error measure between the input target image and the current registered source image is normalized mutual information (NMI). Controls points are moved one at a time by means of gradient descent minimization in order to minimize the error. The gradient is approximated at each control point by means of finite differences.

The B-Spline function that maps the coordinate of the target image to the normalized 2D coordinate of the registered source image is expressed in (1).

$$M_{j0j1} = \sum_{i_{0=0}}^{n_0} \sum_{i_{1=0}}^{n_1} N_{i_0,d_0}\left(\frac{j0}{P0-1}\right) N_{i_1,d_1}\left(\frac{j1}{P1-1}\right) B_{i_0,i_1} \quad (1)$$

Where, the B_{i_0,i_1} values are the control points. $N_{i,d}$ is the basis function, which recursively defines the B-Spline blending function using the Cox de Boor algorithm [7]. n_0, n_1 are the number of the control points along each x, y direction. d_0, d_1 are the degree of the B-Spline curve. $P0$, $P1$ are the x, y image dimensions. $j0, j1$ are the image indices on the target image.

M_{j0j1} contains normalized 2D coordinates (i.e. in unit square) that identify a location in the source image corresponding to the sample at the target image. A measure of error between the source and target images can be computed. The goal is to select the control point positions to make the error measure as small as possible. This is done by moving a single control point at a time using gradient descent. The gradient of the error function is estimated at each control point B_{i_0,i_1}. The gradient at each control point is denoted by (2),

$$\nabla E(i_0, i_1) = \begin{pmatrix} \frac{E(i_0+\Delta x, i_1) - E(i_0-\Delta x, i_1)}{2 \cdot \Delta x}, \\ \frac{E(i_0, i_1+\Delta y) - E(i_0, i_1-\Delta y)}{2 \cdot \Delta y} \end{pmatrix} \quad (2)$$

where, Δx, Δy are sample increments in the target image. The gradient direction is expressed in (3) as a unit length vector,

$$D = \nabla E(i_0, i_1) \,/\, \|\nabla E(i_0, i_1)\| \quad (3)$$

the error measure is computed by moving the control point along the decreasing gradient direction. The point is moved by small steps up to the boundary formed by the neighboring control points until a minimum is found. The error measure function E between the input target image and the current registered source image is NMI.

Figure 3 demonstrates the VOI contour propagation result after applying the B-Spline registration. Slice 7 (the source CED image) is registered with Slice 6 (the target

CED image), and the VOI is copied from the registered slice 7 to slice 6.

2.2. Ball-pivoting and Poisson based surface reconstruction

The semi-automatic prostate segmentation generates VOIs for each axial, sagittal and coronal image. Each VOI contour is generated from the high resolution xy plane. The distance between VOI contours is large due to the low resolution along the z axis on each orthogonal image. We select 100 points to represent each VOI contour and merge the resulting three VOIs in the DICOM space, forming a rough point cloud. The point cloud reflects the high resolution density from each image, and compensates for the low z axis resolution. The Ball-Pivoting and Poisson surface reconstruction algorithms are run against the point cloud to construct the high resolution prostate 3D surface.

We implemented the Ball-Pivoting Algorithm (BPA) [8] in Java, where the BPA is a purely computational geometry based approach. It takes the point cloud as input without normal information to build a rough surface. The algorithm starts by placing a r-ball (a ball of radius r) in contact with three sample points from the point cloud set. Two of the points form an edge, then the algorithm pivots the ball until it touches the third point. The three points form the initial seeding triangle. The r-ball pivots around each edge of the current triangle mesh boundary. When a new point falls into the ball contact range, a new triangle is created. This process repeats until all the points have been considered. A set of triangles is formed while the ball rotates on the surface, constituting the interpolating mesh.

The point cloud merged from the three VOIs has low density sample points due to the low z axis resolution. As a result, the BPA generated mesh will have many holes on the surface. We could re-run the BPA with a larger ball radius as the post-processing hole-filling algorithm to patch the surface. However, we chose the Poisson surface reconstruction algorithm to guarantee the smooth surface and correct surface normal creation.

The Java-based Poisson algorithm (PA) utilizes the implicit function to approximate the surface as a solution to a Poisson equation [9]. PA takes surface points and point normals generated from BPA as input. It partitions the 3D point space into octree based 3D grids. Sparse grids around the non-sample point regions, and smaller dense grids around the sample points. The imported point normals are used as the vector field of the sample point on the small grid. Without the point normals, the sample point vector field can be tri-linear interpolated from the 6 neighbors around the 3D grid. When the vector field is computed, PA splats the vector field to surrounding grid neighbors to remove holes. Then, the key point is to reconstruct the surface by solving the indicator function of the surface M. The 3D indicator function χ is defined as 1 at points inside the surface, and 0 at points outside, as shown in (4).

$$\chi_M(p) = \begin{cases} 1 & if\ p\ inside\ M \\ 0 & if\ p\ outside\ M \end{cases} \quad (4)$$

The gradient of the indicator function is a vector field that is zero almost everywhere, except at points near the surface, where it is equal to the inward surface normal. So, the normal vector field n can be viewed as the gradient of the 'smoothed' indictor function χ_M, where $\nabla\chi_M = n$. Computing the indicator function thus reduces to inverting the gradient operator to find the scalar function χ whose gradient best approximates a vector field n defined by the samples points, i.e. $min_\chi \|\nabla_\chi - n\|$. By applying the divergence operator, the problem transforms to solving Poisson equation (5) for χ.

$$\nabla^2\chi = \nabla \cdot n \quad (5)$$

When the indictor function is solved, a zero-set function is applied to extract the iso-surface.

Figure 4 demonstrates the Ball-Pivoting and Poisson surface reconstruction results respectively. The Java-based open source MIPAV [6] visualization software uploads the final extracted surface in the axial image. Finally, the surface is decimated and saved as a stereolithography(STL) surface file to import into SolidWorks for 3D printing. The BPA and PA combine together to provide a fast and robust model for smooth surface reconstruction.

3. RESULTS

The performance of the semi-automatic segmentation model was evaluated with 45 MRI datasets. We compare the semi-automatic segmentation results with expert manual segmentation. The expert manual segmentation is made by trained researchers and verified by a radiologist. VOI binary masks, VOI volumes and 3D prostate surface volume are used to quantitatively evaluate the segmentation accuracy. The VOIs binary mask method generates the binary mask from VOIs. Then it compares the overlapped region with false negative (FN), false positive (FP), and true positive (TP) volume fractions. The VOI binary masks use the expert manual segmentation as the established truth, Truth Positive (TP) reflects the majority overlapped region between the semi-automatic and manual segmentations. For volumetric measure, the VOIs volume is computed by multiplying the total VOI pixels with a single voxel volume. The 3D surface volume is calculated from the binary surface volumetric mask by multiplying the total surface volumetric voxels with a single voxel volume.

Our proposed method achieves 90% average segmentation accuracy. Figure 5a demonstrates the average volume difference between semi-automatic and the expert manual segmentation. Figure 5b shows the average True Positive overlapped region with the expert's segmentation as the ground truth. The segmentation on axial image

always performs better than the sagittal and coronal images. Figure 6 demonstrates the segmentation results from the registration guided model. The red contours present the semi-automatic segmentation; the green contours present the manual segmentation.

Our proposed segmentation and surface reconstruction model takes under 4 minutes to generate the high resolution 3D prostate surface from thick-sliced MRI images in three orthogonal views. The 3D prostate surface generated from only one view, such as axial view, gives low resolution in the slice direction (z axis) dues to the MRI scan. The axial generated surface always results in a stair-stepping partial volume effect. By merging the axial, sagittal and coronal VOIs contours into a point cloud in DICOM space, the low resolution issue from each orthogonal view's slice direction can be essentially eliminated. The Ball-pivoting and Poisson algorithms finally build a smoothed high resolution 3D prostate surface for 3D mold printing.

The proposed model relies heavily on registration to drive the segmentation algorithm. We also implement 2D OAR registration based method as compared to the 2D gradient descent B-Spline registration based approach. For the OAR parameters, the rotation range is set to between [-20, 20] degree, the rotation step is set to 2 degree; the cost function is correlation ratio; the interpolation for sub-sampling is the cubic B-Spline. For the B-Spline registration, the B-Spline function degree is set to 2, B-Spline number of control point is set to 8; gradient descent min step is set to 1, max step is set to 10; the convergence limitation is 0.05; and the cost function is NMI. Toward the apex and base, the prostate shape is tapered much faster than in the central gland. From experimental results, the OAR method is highly unstable near apex and base as compared to the B-Spline method. The B-Spline parameters are robust to most MRI axial, sagittal and coronal images.

This model is implemented in Java with a stepwise pipeline-based approach (segmentation, surface reconstruction and visualization) under MIPAV software, which is freely available and open-source, and can be obtained from http://mipav.cit.nih.gov.

4. CONCLUSION

A novel method for MRI prostate segmentation, surface reconstruction was presented in this paper. Unlike previous deformation and learning based methods, the proposed model takes advantage of gradient descent B-Spline registration to provide a robust concurrent segmentation mechanism, which is simple, efficient and fast. The BPA and PA surface reconstruction algorithms ensure the rapid prototyping of high resolution 3D prostate surface from thick-slices MRI images at three orthogonal views. The distributed segmentation and reconstruction pipeline provide a unified tool under MIPAV for generating prostate surface model that can be used to improve the correlation of prostate MRI to histopathology [2] and fusion of MRI to TRUS for targeted biopsy [10]. The Java based implementation of the model ensures the wide dissemination to the medical imaging research community. Future work will investigate machine learning based MRI prostate segmentation to improve the segmentation accuracy and to reduce the processing time.

5. REFERENCES

[1] V. Shah, B. Turkbey, H. Mani, Y. Pang, T. Pohida, M. J. Merino, P. Pinto, P. Choyke, M. Bernardo, "Decision support system for localizing prostate cancer based on multiparametric magnetic resonance imaging," *Med Phys*, vol. 39, no. 7, pp. 4093-103, July 2012.

[2] V. Shah, T. Pohida, B. Turkbey, H. Mani, M. Merino, P. Pinto, P. Choyke, M. Bernardo, "A method for correlating in vivo prostate magnetic resonance imaging and histopathology using individualized magnetic resonance-based molds," *Rev Sci Instrument*, vol. 80, pp. 104301, 2009.

[3] N. Betrouni, P. Puech, A. Dewalle, R. Lopes, P. Dubois, M. Vermandel, "3D automatic segmentation and reconstruction of prostate on MR images," *IEEE EMBS*, August, 2007.

[4] J.A. Dowling, K. Shen, P. Raniga, J.P.W. Pluim, P.B. Greer, O. Salvado, J. Fripp, "Patient specific prostate segmentation in 3-D magnetic resonance images," *IEEE Transaction on Medical Imaging*, vol. 31, issue:10, pp. 1955-1964, October, 2012.

[5] Y. Yin, S.V. Fotin, S. Pariaswamy, J. Kunz, H. Haldankar, N. Muradyan, F. Cornud, B. Turkbey, P. Choyke, "Fully automated prostate segmentation in 3D MR based on normalized gradient fields cross-correlation initialization and LOGISMOS refinement," Proc. SPIE 8314, 831406 (2012).

[6] MIPAV, [Medical Image Processing, Analysis, and Visualization (MIPAV)], http://mipav.cit.nih.gov

[7] D. H. Eberly. *3D Game Engine Design: A Practical Approach to Real-Time Computer Graphics*. Morgan Kaufmann, 2007.

[8] F. Bernardini, J. Mittleman, H. Rushmeier, C. Silva, G. Taubin, "The Ball-Pivoting Algorithm for Surface Reconstruction," *IEEE Transactions on Visualization and Computer Graphics*, vol. 5, no. 4, pp. 349-359, Oct.-Dec. 1999.

[9] M. Kazhdan, M. Bolitho, and H. Hoppe, "Poisson surface reconstruction," In *Eurographics Symposium on Geometry Processing*, pp. 61–70, 2006.

[10] S. Xu, J. Kruecker, B. Turkbey, N. Glossop, A. Singh, P. Choyke, P. Pinto, B. Wood, "Real-time MRI-TRUS fusion for guidance of targeted prostate biopsies," *Computer Aided Surg*, vol. 13, no. 5, pp. 255-64, September 2008.

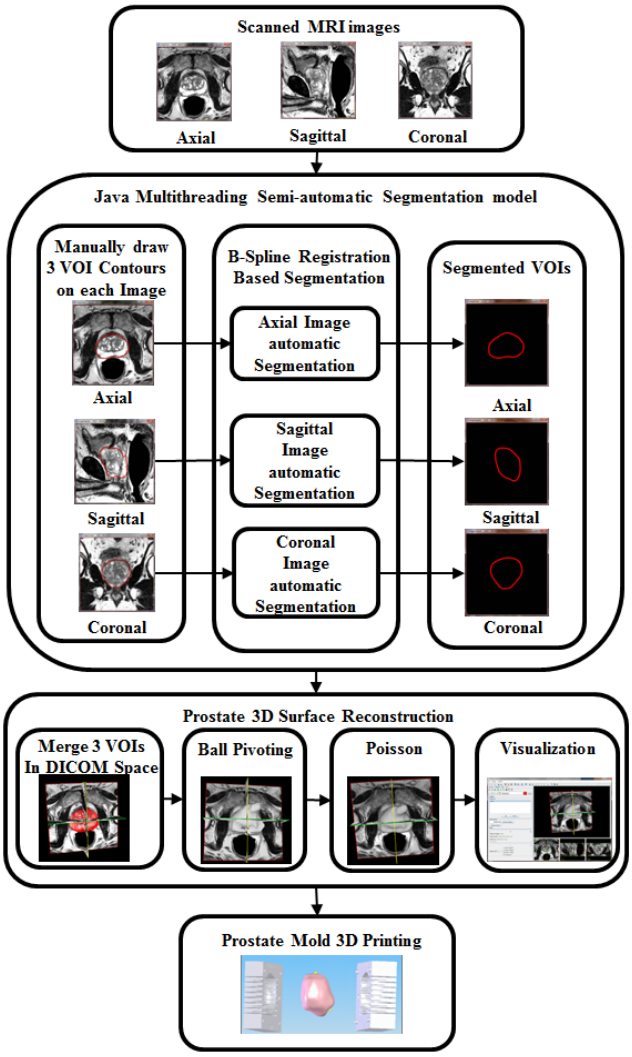

Figure 1. Schematic representation of segmentation and surface reconstruction model from prostate MRI images

Figure 2. Registration guided automatic segmentation model

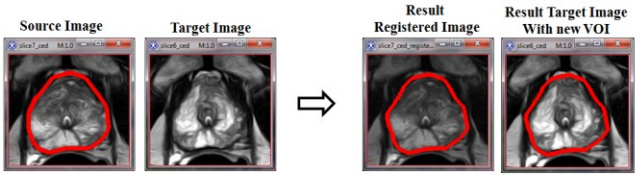

Figure 3. VOI contour propagation result after B-Spline registration from CED slice 7 to 6.

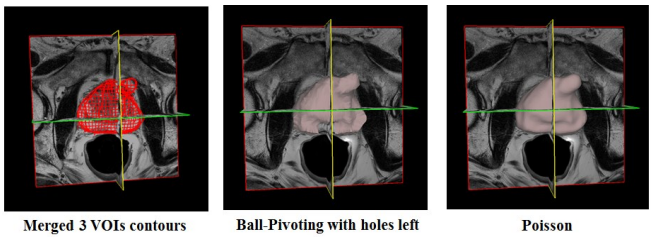

Figure 4. Ball-Pivoting and Poisson surface reconstruction

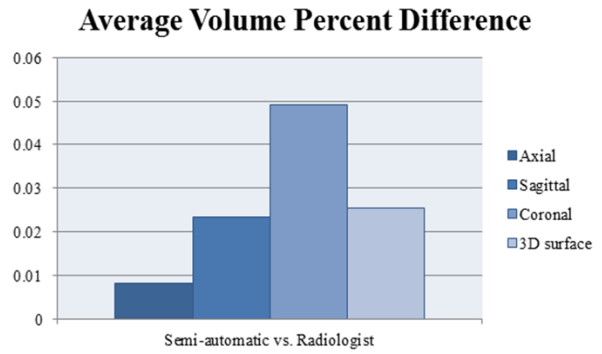

(a)VOIs volume difference

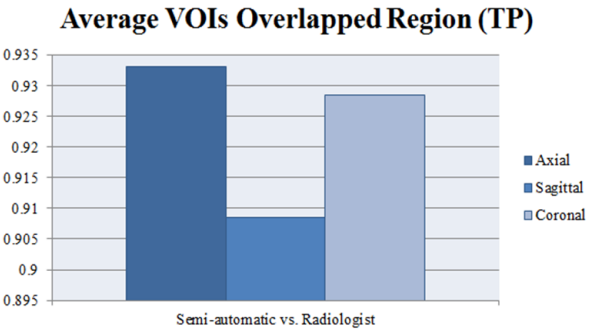

(b) VOIs overlapped region

Figure 5. Segmentation performance evaluation

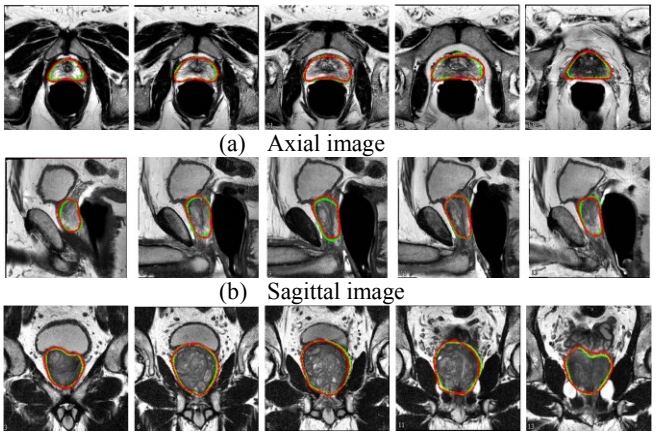

(a) Axial image

(b) Sagittal image

(c) Coronal image

Figure 6. Registration guided model segmentation results